HHS Public Access

Author manuscript

Phys Rev Appl. Author manuscript; available in PMC 2019 October 02.

Published in final edited form as:

Phys Rev Appl. 2018 February ; 9(2): . doi:10.1103/PhysRevApplied.9.024008.

Strong Polarization Transformation of Bloch Surface Waves

Junxue Chen[1], **Douguo Zhang**[2,*], **Pei Wang**[2], **Hai Ming**[2], **Joseph R. Lakowicz**[3]

[1]School of Science, Southwest University of Science and Technology, Mianyang, Sichuan 621010, China

[2]Institute of Photonics, Department of Optics and Optical Engineering, University of Science and Technology of China, Hefei, Anhui 230026, China

[3]Center for Fluorescence Spectroscopy, Department of Biochemistry and Molecular Biology, University of Maryland School of Medicine, Baltimore, Maryland 21201, United States

Abstract

Polarization is an intrinsic attribute of optical waves, so manipulating the polarization state of optical surface waves can be of a fundamental importance for the next-generation information and bio-photonics technology. Here, we show theoretically that the polarization of the Bloch surface wave (BSW) on a dielectric multilayer can be transformed between a transverse-electric (TE) state and a transverse-magnetic (TM) state by using the laterally continuous grooves inscribed on this multilayer. This polarization transformation can be enhanced or inhibited by the interference between the reflected BSW beams, which can be tuned by the periodicity and depth of the grooves. The maximum polarization transformation efficiency can be achieved as high as 43% when the number of grooves is increased to 10. A generalized Fresnel formula is proposed to describe the polarization transformation of the BSW beams. Due to this polarization transformation, an anomalous reflection of BSW beams can be realized, which is the inequality between the incident angle and the reflection angle.

I. INTRODUCTION

Bloch surface waves (BSWs), the electromagnetic surface waves excited at the interface between a truncated periodic dielectric multilayer with a photonic band gap (PBG) and its surrounding medium, have been considered as the dielectric analogue of surface plasmon polaritons (SPPs) that are also the electromagnetic surface waves but propagating at the interface between a metallic film and its dielectric cladding [1–2]. Similar as the SPPs, BSWs can also induce the optical near-field confinement and enhancement, and can have larger wave-vectors than light of the same frequency in vacuum. BSWs have been applied in nanoscale optical waveguides, sensing, fluorescence emission enhancement or sorting, surface enhanced Raman scattering, and so on [3–13]. It also can realize the giant Goos-Hanchen shift, which will improve the functionality of sensors and may have an impact on the further development of sensor technology [14]. The BSWs are not subject to losses caused by absorption in metal, which allows for BSW with a high resonance quality factor

* dgzhang@ustc.edu.cn.

and a long propagation length. There are many choices of the dielectric materials for BSWs, which allows this dielectric multilayer to be used from deep ultraviolet (UV) to near-infrared (NIR) wavelengths [15]. For SPPs, it can only be sustained in transverse magnetic (TM) polarization state [16–19], whereas the BSWs can be of either transverse electric (TE) or TM polarization. Previously, most work on BSWs are related with the TE polarized BSW [3–11, 20], but few on the TM polarized one [12, 13]. The reason is that the generation of TM polarized BSWs is always affected by the Brewster angle effect [21]. There are no reports on energy coupling between the TE and TM polarized BSW, or reports on how to transform the TE polarized BSW into TM one and vice versa. Polarization is one of the basic parameters for optical waves, hence the ability to manipulate the polarization state of the electromagnetic surface waves can be of a fundamental importance for both science and technology. For example, it can increase the information capacity with a new parameter (polarization) involved in the surface waves, similar as the applications of cylindrical vector beams or orbital angular momentum in optical communications [22, 23]. It can also introduce different light-matter interactions between electromagnetic surface waves and polarization sensitive materials or cells. Although 3D waveguide based polarization rotators are routinely used in modern photoelectric components and provide nearly unitary efficiency of polarization transformation [24, 25], we have not seen any reports on the polarization rotators for 2D surface waves.

II. THE DISPERSION RELATIONS OF BSW

The proposed dielectric multilayer that sustains both TE and TM polarized BSWs is consisted of 18 alternating dielectric layers of Si_3N_4 and SiO_2 as shown in Fig. 1(a). The refractive indices of Si_3N_4 and SiO_2 layers are 2.65 and 1.48, respectively. The thickness of Si_3N_4 and SiO_2 layers are fixed at 80 nm and 126 nm, respectively. The thickness of the top SiO_2 layer can be varied and denoted as h. A rectangular groove with width w_g and depth h_g is inscribed on the top SiO_2 layer. A BSW is obliquely incident on the groove. The symbols θ_i, θ_r and θ_t denote the incidence, reflection and transmission angles of BSW, respectively. Different from the SPPs supported by the metal film, the dielectric multilayer can support the propagation of TE-BSW (the electric field perpendicular to X-Z plane) and TM-BSW (the magnetic perpendicular to the X-Z plane). Moreover, the propagation of BSW is sensitive to the top layer's thickness h as shown in the inset of Fig. 1(b). Figure 1(b) demonstrates the change of the effective refractive indices of TE-BSW and TM-BSW modes as a function of the top layer's thickness h. The effective refractive indices of TE-BSW and TM-BSW modes decrease with the decreasing of the thickness h. Compared with the case of TE-BSW modes, the TM-BSW modes can be sustained by dielectric multilayer in a very limited thickness range, which is attributed to that the bandgap width of dielectric multilayer for TM polarization is much smaller than that for TE polarization due to the Brewster effect of TM polarization. The photonic bandgap of the dielectric multilayer and the dispersion relations for TE-BSW and TM-BSW modes are shown in Figs. 2(a) and 2(b), respectively. The yellow zone denotes the photonic stop band of dielectric multilayer. As the top layer's thickness is fixed at 320 nm, the dispersion curves for TE_0-BSW and TM_1-BSW are also shown in Figs. 2(a) and 2(b), respectively. It is noted that the dispersion curve for TM_1-BSW can be held in a very limited frequency range due to the narrow bandgap. To understand the

waveguiding behaviors of BSW, the field distributions for TE_0-BSW and TM_1-BSW are shown in Figs. 2(c) and 2(d), respectively. A node of field for TM_1-BSW can be observed in the top's layer, but there is no node in the top's layer for TE_0-BSW. It is the reason that the mode is named according to the number of field node in the top's layer of dielectric multilayer. In addition, the penetration depth of TM_1-BSW in the dielectric multilayer is larger than that of TE_0-BSW due to the narrow bandgap. As noted in Fig. 1(b), the dielectric multilayer can sustain the TE_0-BSW and TM_1-BSW modes with the thickness h ranging from 300 nm to 500 nm.

III. POLARIZATION TRANSFORMATION OF BSW

A. The case of the single groove

Here, a groove was fabricated on the dielectric multilayer as shown in Fig. 1(a). As the BSW is obliquely incident on the groove, the interpolarization coupling between TE-BSW and TM-BSW occurs due to the discontinuous of the interface, besides the partial reflection and transmission of BSW. The reflection, transmission and polarization transformation intensities of TE_0-BSW and TM_1-BSW as a function of the incidence angle are shown in Figs. 3(a) and 3(b), respectively. The results are obtained by mode-matching method [26, 27]. The validity of mode-matching method is confirmed by comparing with the results obtained from the finite difference frequency domain (FDFD) method [28]. The detailed descriptions of the simulation process are given in the Supplemental Material [29]. If the incident wave is TE_0-BSW, R_{ss} and T_{ss} denote the reflection and transmission intensities of TE_0-BSW, R_{sp} and T_{sp} denote the reflection and transmission intensities of TM_1-BSW which are excited by the incident TE_0-BSW. Similarly, if the incident wave is TM_1-BSW, R_{pp} and T_{pp} denote the reflection and transmission intensities of TM_1-BSW, R_{ps} and T_{ps} denote the reflection and transmission intensities of TE_0-BSW excited by the TM_1-BSW. To facilitate the comparison of the polarization transformation efficiency of BSW, the intensities of R_{sp}, R_{ps}, T_{sp} and T_{ps} are magnified by a factor of 10 in the curves shown in Figs. 3(a) and 3(b).

As the BSW propagates across the groove, the reflection and transmission of BSW are well related to the difference of effective refractive indices of BSW inside and outside of the groove. Because the effective refractive index of TE_0-BSW is larger than that of TM_1-BSW for the same top layer's thickness, the reflection and transmission curves of TE_0-BSW demonstrate much more drastic changes at the large incidence angle. For example, as the incidence angle of TE_0-BSW is larger than 50°, the reflection intensity of TE_0-BSW is dramatically increased with the increasing of the incidence angle, and finally approaches one as shown in Fig. 3(a). The polarization transformation R_{sp} from TE_0-BSW to TM_1-BSW is firstly increased with the increasing of the incidence angle, but finally disappears around 55° due to the total internal reflection of TM_1-BSW, which is determined by matching the transverse wavevector.

$$k_0 n_{eff,BSW}^{TE_0} \sin\theta_i = k_0 n_{eff,BSW}^{TM_1} \sin\theta_r \quad (1)$$

where $n_{eff,BSW}^{TE_0}$ and $n_{eff,BSW}^{TM_1}$ are the effective refractive indices of TE_0-BSW and TM_1-BSW, respectively. Because the effective refractive index of TM_1-BSW is smaller than that of TE_0-BSW, the total internal reflection angle of TM_1-BSW is expressed as: $\theta_c^{TM_1} = arc\sin\left(n_{eff,BSW}^{TM_1}/n_{eff,BSW}^{TE_0}\right)$. In contrast, as the incident BSW is TM_1-BSW, the total internal reflection cannot occur, and the reflected angle of TE_0-BSW excited by TM_1-BSW can be expressed as: $\theta_r^{TE_0} = arc\sin\left(n_{eff,BSW}^{TM_1}\sin\theta_i/n_{eff,BSW}^{TE_0}\right)$. There will be two reflected beams propagating along different directions due to the different effective refractive indices for TE_0-BSW and TM_1-BSW at the same top layer's thickness, as the BSW is obliquely incident on the groove. Besides the incidence angle, the depth and width of groove can also affect the polarization transformation efficiency of BSW. The influences of the depth and width of groove to the polarization transformation efficiency of TE_0-BSW are shown in Fig. 4.

To evaluate the polarization transformation efficiency of TE_0-BSW, the scattering loss of TE_0-BSW is defined as:

$$S_{loss} = 1 - R_{ss} - T_{ss} - R_{sp} - T_{sp} \quad (2)$$

As the width of groove is fixed at 400 nm, the polarization transformation intensity R_{sp} and the scattering loss S_{loss} of TE_0-BSW versus the depth of groove and incidence angle are shown in Figs. 4(a) and 4(b), respectively. With the increasing of the depth of groove, the R_{sp} is increased, but the S_{loss} of BSW is also increased. To balance the efficiency of polarization transformation and the scattering loss of BSW, the depth of groove is chosen to be 150 nm. In addition, the relationship of polarization transformation intensity R_{sp} and the scattering loss S_{loss} of BSW between the width of groove and incidence angle are shown in Figs. 4(c) and 4(d), respectively. As the width of groove is larger than 200 nm, the polarization transformation of BSW becomes insensitive to the changes of groove depth. Moreover, the scattering loss of BSW will increase as the width of groove is larger than 500 nm. Therefore, the depth and width of groove are chosen as 150 nm and 400 nm in simulation to balance the efficiency of polarization transformation and the scattering loss of BSW.

B. The case of the two grooves

If multiple grooves are fabricated on the dielectric multilayer, this polarization transformation between TE_0-BSW and TM_1-BSW can be enhanced or inhibited by the interference effect of multiple beams. As noted in Fig. 5, the two grooves are introduced into the structure, the separation distance between grooves is denoted as L_d. Figures 5(a) and 5(b) demonstrate the reflection, transmission and polarization transformation intensities of BSW as a function of incidence angle. Compared to the case of the single groove, the reflection and transmission intensities of the TE_0-BSW exhibit a sharp dip and peak around incidence angle of 66°, respectively. When the incidence angle of TE_0-BSW is larger than 60°, the single groove demonstrates the strong reflection to the TE_0-BSW as shown in the Fig. 3(a).

The groove is similar to a 2D partially reflecting mirror for the TE_0-BSW. The two grooves with separation distance L_d can act as an 2D Fabry-Perot (FP) cavity, which contributes to the strongly changes of reflection and transmission for TE_0-BSW. Furthermore, the polarization transformation intensity R_{sp} (from TE_0-BSW to TM_1-BSW during reflection) is about increased by 5-fold compared to the case of the single groove as noted in Fig. 3(a). Similarly, the enhanced polarization transformation intensity R_{ps} (from TM_1-BSW to TE_0-BSW during reflection) is also observed in the Fig. 5(b).

IV. DISCUSSIONS

A. Generalized Fresnel formula for polarization transformation of BSW

The enhanced polarization transformation of BSW is attributed to the multiple reflection of BSW in the two grooves. To describe the physical process of polarization transformation of BSW modes in the two grooves in detail, the Fresnel formula for the multilayer film is generalized to deal with the reflection and transmission of the BSW crossing the grooves. The groove can be considered as an equivalent interface. As the BSW propagates across the equivalent interface, the reflection, transmission and polarization transformation of BSW occur. A simplified model for multiple reflections of BSW between the two grooves is demonstrated in the inset of Fig. 6. The structure is then divided into three parts by two equivalent interfaces. The three parts of structure are numbered as 0, 1 and 2, respectively. The BSW is launched at the region 0. As the TE_0-BSW propagates from region *i* to region *j*, r_{ij}^{ss} and t_{ij}^{ss} denote the reflection and transmission coefficients of TE_0-BSW, respectively. r_{ij}^{sp} and t_{ij}^{sp} denote the polarization transformation coefficients of TE_0-BSW to TM_1-BSW, respectively. Similarly, as the TM_1-BSW transmits from region *i* to region *j*, the terms r_{ij}^{pp}, t_{ij}^{pp}, r_{ij}^{ps} and t_{ij}^{ps} are used to denote the reflection, transmission and polarization transformation coefficients of TM_1-BSW, respectively. From the simplified model and the defined coefficients, the generalized Fresnel formula of BSW can be expressed as:

$$\begin{pmatrix} A_s^r \\ A_p^r \end{pmatrix} = \left(\tilde{\boldsymbol{R}} + \boldsymbol{MS}\tilde{\boldsymbol{T}}\right)\begin{pmatrix} A_s^i \\ A_p^i \end{pmatrix} \quad (3)$$

where A_s^i and A_p^i denote the amplitude of the incident TE_0-BSW and TM_1-BSW, respectively. A_s^r and A_p^r denote the amplitude of the reflected TE_0-BSW and TM_1-BSW, respectively. As the BSW propagates across the two grooves, the reflection and polarization transformation coefficients of BSW can be defined:

$$r_{012}^{ss} = \left.\frac{A_s^r}{A_s^i}\right|_{A_p^i=0}, \quad r_{012}^{sp} = \left.\frac{A_p^r}{A_s^i}\right|_{A_p^i=0}, \quad r_{012}^{ps} = \left.\frac{A_s^r}{A_p^i}\right|_{A_s^i=0}, \quad r_{012}^{pp} = \left.\frac{A_p^r}{A_p^i}\right|_{A_s^i=0} \quad (4)$$

In Eq. (3), the terms $\widetilde{\mathbf{R}}$ and $\tilde{\boldsymbol{T}}$ denote the matrix of reflection and transmission coefficients at the first groove, i.e. the first equivalent interface.

$$\widetilde{\mathbf{R}} = \begin{pmatrix} r_{01}^{ss} & r_{01}^{ps} \\ r_{01}^{sp} & r_{01}^{pp} \end{pmatrix}, \quad \tilde{\boldsymbol{T}} = \begin{pmatrix} t_{01}^{ss} & t_{01}^{ps} \\ t_{01}^{sp} & t_{01}^{pp} \end{pmatrix} \quad (5)$$

The matrix $\boldsymbol{M}$ and $\boldsymbol{S}$ describe the multiple reflection of BSW between the two equivalent interfaces.

$$\boldsymbol{M} = \begin{pmatrix} t_{10}^{ss} r_{12}^{ss} e^{2i\gamma_s L_d} + t_{10}^{ps} r_{12}^{sp} e^{i(\gamma_s+\gamma_p)L_d} & t_{10}^{ss} r_{12}^{ps} e^{i(\gamma_s+\gamma_p)L_d} + t_{10}^{ps} r_{12}^{pp} e^{2i\gamma_p L_d} \\ t_{10}^{sp} r_{12}^{ss} e^{2i\gamma_s L_d} + t_{10}^{pp} r_{12}^{sp} e^{i(\gamma_s+\gamma_p)L_d} & t_{10}^{sp} r_{12}^{ps} e^{i(\gamma_s+\gamma_p)L_d} + t_{10}^{pp} r_{12}^{pp} e^{2i\gamma_p L_d} \end{pmatrix} \quad (6)$$

$$\boldsymbol{S} = \begin{pmatrix} 1 - r_{10}^{ss} r_{12}^{ss} e^{2i\gamma_s L_d} - r_{10}^{ps} r_{12}^{sp} e^{i(\gamma_s+\gamma_p)L_d} & -r_{10}^{ss} r_{12}^{ps} e^{i(\gamma_s+\gamma_p)L_d} - r_{10}^{ps} r_{12}^{pp} e^{2i\gamma_p L_d} \\ -r_{10}^{sp} r_{12}^{ss} e^{2i\gamma_s L_d} - r_{10}^{pp} r_{12}^{sp} e^{i(\gamma_s+\gamma_p)L_d} & 1 - r_{10}^{sp} r_{12}^{ps} e^{i(\gamma_s+\gamma_p)L_d} - r_{10}^{pp} r_{12}^{pp} e^{2i\gamma_p L_d} \end{pmatrix}^{-1} \quad (7)$$

Here, the terms $\gamma_s = \sqrt{k_0^2 \left(n_{eff,BSW}^{TE_0}\right)^2 - k_y^2}$ and $\gamma_p = \sqrt{k_0^2 \left(n_{eff,BSW}^{TM_1}\right)^2 - k_y^2}$ are the longitudinal wavenumber of TE_0-BSW and TM_1-BSW along the X axis, respectively. k_y is the transverse wavenumber of BSW along the Y axis. Then, the reflection intensities R_{ss} and R_{pp} can be expressed as:

$$R_{ss} = \left| r_{012}^{ss} \right|^2, \quad R_{pp} = \left| r_{012}^{pp} \right|^2 \quad (8)$$

The polarization transformation intensities R_{sp} and R_{ps} are given by:

$$R_{sp} = \left| r_{012}^{sp} \right|^2 \frac{P_{x,r}^{TM_1}}{P_{x,in}^{TE_0}}, \quad R_{ps} = \left| r_{012}^{ps} \right|^2 \frac{P_{x,r}^{TE_0}}{P_{x,in}^{TM_1}} \quad (9)$$

The terms $P_{x,r}^{*}$ and $P_{x,in}^{*}$ denote the propagation power along the X axis for the reflected and incident BSW modes, respectively.

Figure 6(a) demonstrates the polarization transformation coefficient r_{012}^{sp} for the TE_0-BSW propagating across two grooves versus the incidence angle. The solid line denotes the results obtained from the generalized Fresnel formula shown in Eq. (4), and the triangles denote the

results obtained from the mode-matching method. To facilitate the comparison of the polarization transformation enhanced by two grooves, the transformation coefficient r^{sp} of TE_0-BSW for a single groove is also shown in the Fig. 6(a) with a dotted line. It is noted that the transformation coefficient r_{012}^{sp} of TE_0-BSW can be enhanced or inhibited at the certain incidence angle relative to the coefficient r^{sp}, which is attributed to the interference effect between the multiple beams. Similarly, the polarization transformation coefficient r_{012}^{ps} for the TM_1-BSW propagating across two grooves versus the incidence angle is shown in Fig. 6(b). Compared to the transformation coefficient r^{ps} for a single groove, the coefficient r_{012}^{ps} can also be enhanced or inhibited at the certain incidence angle due to the interference effect from the reflected beams. The interference effects are sensitive to the phase factors of the reflected beam, which are well related to the wavenumber γ_s, γ_p and the separation distance L_d noted in Eq. (6) and Eq. (7). Then, this is a practical way to control the polarization transformation of BSW by adjusting the separation distance L_d between the grooves.

B. Anomalous reflection of BSW

As the TE_0-BSW propagates across the two grooves, Figures 7(a) and 7(b) demonstrates the polarization transformation intensity R_{sp} and the reflection intensity R_{ss} as a function of the incidence angle and the separation distance L_d, respectively. With the increasing of the separation distance L_d, the R_{sp} and R_{ss} exhibit the periodic changes arising from the constructive and destructive interference of reflected BSW beams. Furthermore, the changes of R_{sp} and R_{ss} demonstrate the different periodicity due to the different interference effect noted in Eq. (6) and Eq. (7). It is feasible to achieve the completely polarization transformation in the reflected beam by adjusting the distance L_d, such as the point P1 labeled in Figs. 7(a) and 7(b). The point P1 means that the incidence angle of TE_0-BSW is 50.6°, and the separation distance L_d is 410 nm. The R_{sp} can achieve the maximum value, and the value of R_{ss} can become the minimum at this condition denoted by point P1. The electric field distribution of structure is calculated by mode-matching method at this condition, as shown in Fig. 7(c). The electric fields are extracted at the location z= 10 nm (X-Y plane). The incident TE_0-BSW beam is modeled as the Gaussian shape with half width 10λ. λ= 633 nm is the incident wavelength. An interesting phenomenon is observed in the Fig. 7(c). The reflection angle of beam relative to the normal direction of the grooves is larger than the incident angle due to the excitation of TM_1-BSW. The reflection angle of beam can be predicted from the Eq. (1), and is equal to 70.4°. This anomalous reflection is attributed to the polarization transformation of BSW, which is different from that arising from a metasurface or metagratings [30–33]. Then, the grooves can be used as the mode converter or polarization rotator for BSWs.

In addition, the generation of TM_1-BSW can also be inhibited by changing the distance L_d. For example, as the distance L_d is increased to 680 nm, the value of R_{sp} can becomes minimal due to the destructive interference of beams, but the value of R_{ss} is increased corresponding to the point P2 labeled in Figs. 7(a) and 7(b). At this condition, the total electric field distribution is calculated and shown in Fig. 7(d). In this case, the structure demonstrates the normal reflection. The reflection angle of beam is equal to the incident angle. The polarization of reflection beam is the same as that of incident beam. Therefore,

the separation distance L_d between the grooves is an efficient parameter to control the polarization transformation of BSW.

C. The effect of the multiple grooves

Moreover, it is noted that most of the energy of TE_0-BSW can also transmit across the grooves as shown in Fig. 7(c). This part of energy can be further transformed to that of TM_1-BSW by increasing the reflection of TE_0-BSW, which can be achieved by increasing the number of the grooves. Figure 8(a) demonstrates the polarization transformation intensity R_{sp} versus the incidence angle with different number of grooves. The separation distance L_d between grooves is fixed at 400 nm. It is noted that the peak value of polarization transformation intensity R_{sp} around 50.6° is enhanced with the increasing of the number of grooves. As the distance L_d is increased to 680 nm, the constructive interference condition of polarization transformation R_{sp} is changed to 45.8°. With the increasing of the number of grooves, the peak value of polarization transformation intensity R_{sp} around 45.8° is also enhanced, which is shown in Fig. 8(b). To evaluate the maximum value of R_{sp} achieved by the multiple grooves, the peak values of R_{sp} at the different distance L_d versus the number of grooves are shown in Fig. 8(c). It is noted the values of R_{sp} can approach the stable values as the number of grooves N_g is larger than 10. The maximum polarization transformation efficiency of TE_0-BSW to TM_1-BSW achieved by the multiple grooves can approach 43%.

V. CONCLUSION

In conclusion, the polarization transformation between the TE and TM polarized BSW was achieved for the first time, which is through the multiple reflections from the grooves inscribed on a dielectric multilayer. By tuning the depth of groove and the separation distance between grooves, the polarization transformation efficiency can be reached as high as 43% attributed from the constructive interference of reflected beams. This value is much larger than the case of surface waves to free-space waves [34], where the transformation efficiency is only 0.4 %. And also, to the best of our knowledge, we have not noticed the reports on the polarization transformation of any surface waves. Due to this polarization transformation between the two polarized BSWs, an anomalous reflection phenomenon appears that the reflection angle of beam is different from the incidence angle. This phenomenon is different from the anomalous reflection induced by the widely investigated metasurfaces and provides a new means to manipulate the polarization and reflection of the electromagnetic waves [30–33]. Furthermore, the polarization transformation of BSW can be adjusted by changing the separation distance between grooves. This provides a feasible way to strengthen or inhibit the polarization transformation of BSW in the on-chip optical circuit system. The proposed method for polarization transformation not only can be used in the dielectric multilayer for BSWs, it is also applicable for the planar waveguide that containing two waveguide modes of different polarization states [35]. Our work will have potential applications in various areas, such as lab-on-a-chip devices, bio-sensing or imaging along with others. We have already reported that the different penetration depths above the surface can be used for selective sensing from the surface and bulk volume regions of the samples [35].

ACKNOWLEDGEMENTS

This work was supported by MOST (2013CBA01703 and 2016YFA0200601), NSFC (61427818 and 11374286), the Science and Technological Fund of Anhui Province for Outstanding Youth (1608085J02) and the Longshan academic talent research supporting program of SWUST (17LZX626). This work was also supported by grants from the National Institute of Health (GM107986, EB006521, EB018959, and OD019975).

References

1. Meade RD, Brommer KD, Rappe AM, and Joannopoulos JD, Electromagnetic Bloch Waves at The Surface of A Photonic Crystal, Phys. Rev. B 44,44–49 (1999).
2. Yeh P, Yariv A, and Hong CS, Electromagnetic Propagation in Periodic Stratified Media. I. General Theory, J. Opt. Soc. Am 67, 423 (1977).
3. Sinibaldi A, Danz N, Descrovi E, Munzert P, Schulz U, Sonntag F, Dominici L, and Michelotti F, Direct Comparison of the Performance of Bloch Surface Wave and Surface Plasmon Polariton Sensors, Sens. Actuat. B-Chem 174, 292–298 (2012).
4. Badugu R, Nowaczyk K, Descrovi E, and Lakowicz JR, Radiative Decay Engineering 6: Fluorescence on One-Dimensional Photonic Crystals, Anal. Biochem 442, 83–96 (2013). [PubMed: 23896462]
5. Toma K, Descrovi E, Toma M, Ballarini M, Mandracci P, Giorgis F, Mateescu A, Jonas U, Knoll W, and Dostalek J, Bloch-Surface Wave-Enhanced Fluorescence Biosensor, Biosens. Bioelectron 43,108–114 (2013). [PubMed: 23291217]
6. Pirotta S, Xu XG, Delfan A, Mysore S, Maiti S, Dacarro G, Patrini M, Galli M, Gutzzetti G, Bajoni D, Sipe JE, Walker GC and Liscidini M, Surface-Enhanced Raman Scattering in Purely Dielectric Structures *via* Bloch Surface Waves, J. Phys. Chem. C 117,6821–6825 (2013).
7. Descrovi E, Sfez T, Quaglio M, Brunazzo D, Dominici L, Michelotti F, Herzig HP, Martin OJF, and Giorgis F, Guided Bloch Surface Waves on Ultrathin Polymeric Ridges, Nano Lett 10, 2087–2091 (2010). [PubMed: 20446750]
8. Angelini A, Lamberti A, Ricciardi S, Frascella F, Munzert P, De Leo N, and Descrovi E, In-Plane 2D Focusing of Surface Waves by Ultrathin Refractive Structures, Opt. Lett 39, 6391–6393 (2014). [PubMed: 25490476]
9. Angelini A, Lamberti A, Ricciardi S, Frascella F, Munzert P, De Leo N, and Descrovi E, In-Plane 2D Focusing of Surface Waves by Ultrathin Refractive Structures, Opt. Lett 39, 6391–6393 (2014). [PubMed: 25490476]
10. Angelini A, Barakat E, Munzert P, Boarino L, De Leo N, Enrico E, Giorgis F, Herzig HP, Pirri CF, and Descrovi E, Focusing and Extraction of Light Mediated by Bloch Surface Waves, Sci. Rep 4,5428 (2014). [PubMed: 24962615]
11. Angelini A, Munzert P, Enrico E, De Leo N, Scaltrito L, Boarino L, Giorgis F, and Descrovi E, Surface-Wave-Assisted Beaming of Light Radiation from Localized Sources, ACS Photonics 1, 612–617 (2014).
12. Sinibaldi A, Fieramosca A, Rizzo R, Anopchenko A, Danz N, Munzert P, Magistris C, Barolo C, and Michelotti F, Combining Label-Free and Fluorescence Operation of Bloch Surface Wave Optical Sensors, Opt. Lett 39, 2947–2949 (2014). [PubMed: 24978244]
13. Gao J, Sarangan AM, and Zhan Q, Polarization Multiplexed Fluorescence Enhancer using a Pixelated One-Dimensional Photonic Band Gap Structure, Opt. Lett 37, 2640–2642 (2012). [PubMed: 22743480]
14. Soboleva V, Moskalenko VV, and Fedyanin AA, Giant Goos-Hänchen Effect and Fano Resonance at Photonic Crystal Surfaces, Phys. Rev. Lett 108, 123901 (2012). [PubMed: 22540582]
15. Badugu R, Mao JY, Blair S, Zhang DG, Descrovi E, Angelini A, Huo YP, and Lakowicz JR, Bloch Surface Wave-Coupled Emission at Ultraviolet Wavelengths, J. Phys. Chem C 120, 28727–28734 (2016).
16. Maier SA, Plasmonics: Fundamentals and Applications (Springer: New York, 2007).
17. Raether H, Surface Plasmons on Smooth and Rough Surfaces and on Gratings (Springer-Verlag Berlin Heidelberg, 1988).

18. Lin J, Dellinger J, Genevet P, Cluzel B, de Fornel F, and Capasso F, Cosine-Gauss Plasmon Beam: A Localized Long-Range Nondiffracting Surface Wave, Phys. Rev. Lett 109, 093904 (2012). [PubMed: 23002838]
19. Bharadwaj P, Bouhelier A, and Novotny L, Electrical Excitation of Surface Plasmons, Phys. Rev. Lett 106, 226802 (2011). [PubMed: 21702623]
20. Yu L, Barakat E, Sfez T, Hvozdara L, Di Francesco J, and Herzig HP, Manipulating Bloch Surface Waves In 2D: A Platform Concept-Based Flat Lens, Light: Sci. Appl 3, 124 (2014).
21. Born M and Wolf E, Principles of Optics, 7th edition (Cambridge University Press 1999).
22. Zhan QW, Cylindrical vector beams: from mathematical concepts to applications, Adv. Opt. Photonics 1, 1–57 (2009).
23. Yao AM and Padgett MJ, Orbital angular momentum: origins, behavior and applications, Adv. Opt. Photonics 3, 161–204 (2011).
24. Alferness RC and Buhl LL, Waveguide electro-optic polarization transformer, Appl. Phys. Lett 38, 655–657 (1981).
25. Heidrich H, Albrecht P, Hamacher M, Nolting HP, Schroeter-Janssen H, and Weinert CM, Passive mode converter with a periodically tilted InP/GaInAsP rib waveguide, IEEE photonics tech. Lett 4, 34–36 (1992).
26. Derudder H, Olyslager F, De Zutter D, and Van den Berghe S, Efficient mode-matching analysis of discontinuities in finite planar substrates using perfectly matched layers, IEEE T. Antenn. Propag 49, 185–195 (2001).
27. Bienstman P, Rigorous and efficient modelling of wavelength scale photonic components, Ph.D. thesis, Ghent University, (2001).
28. Rumpf RC, Design and optimization of nano-optical elements by coupling fabrication to optical behavior, Ph.D. thesis, University of Central Florida, (2006).
29. See Supplemental Material at for more discussions on the simulation details using FDFD method.
30. Yu NF and Capasso F, Flat Optics with Designer Metasurfaces, Nat. Mater 13,139–150 (2014). [PubMed: 24452357]
31. Kildishev AV, Boltasseva A, and Shalaev VM, Planar Photonics with Metasurfaces, Science 339, 1232009 (2013). [PubMed: 23493714]
32. Yu N, Genevet P, Kats MA, Aieta F, Tetienne JP, Capasso F, and Gaburro Z, Light Propagation with Phase Discontinuities: Generalized Laws of Reflection and Refraction, Science 334, 333–337 (2011). [PubMed: 21885733]
33. Ra'di Y, Sounas DL, and Alù A, Metagratings: Beyond the Limits of Graded Meta surfaces for Wave Front Control, Phys. Rev. Lett 119, 067404 (2017). [PubMed: 28949646]
34. Stegeman GI, Glass NE, Maradudin AA, Shen TP, and Wallis RF. Fresnel relations for surface polaritons at interfaces. Opt. Lett 8, 626–628 (1983). [PubMed: 19718205]
35. Wang R, Zhang D, Zhu L, Wen X, Chen J, Kuang C, Liu X, Wang P, Ming H, Badugu R, and Lakowicz JR, Selectable Surface and Bulk Fluorescence Imaging with Plasmon-Coupled Waveguides, J. Phys. Chem C 119, 22131–22136 (2015).

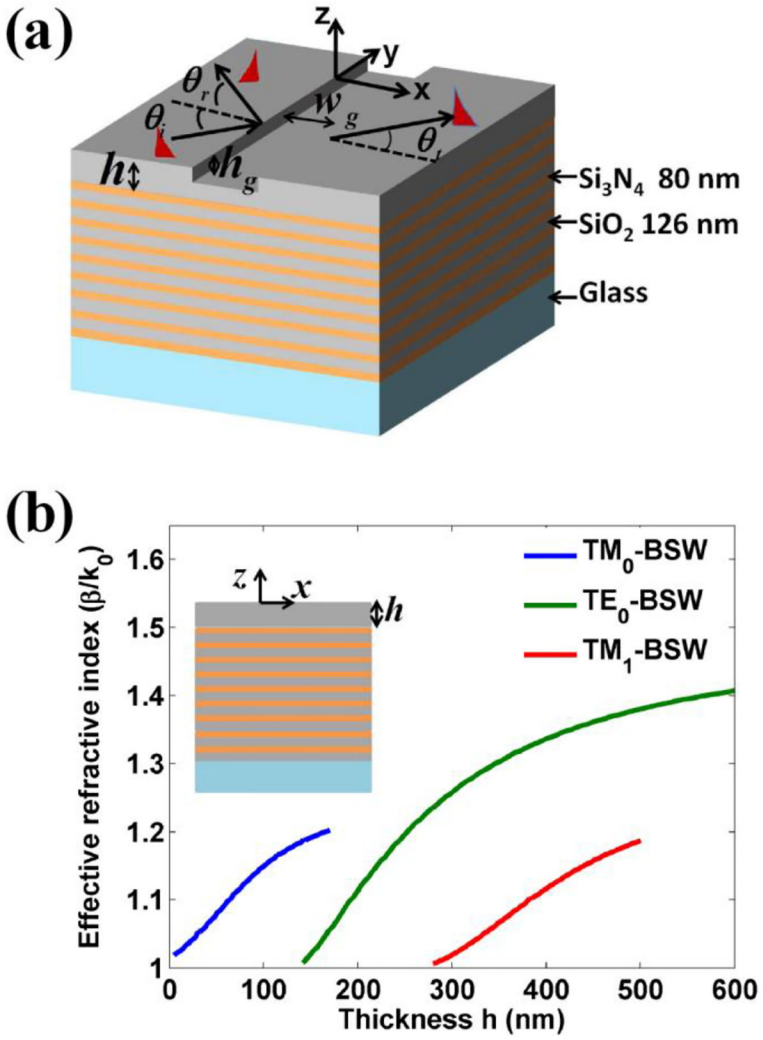

FIG. 1.

(a) Schematic illustration of the dielectric multilayer. The dielectric multilayer is consisted of 18 alternating dielectric layers of Si_3N_4 (80-nm-thick) and SiO_2 (126-nm-thick). The thickness of top SiO_2 layer can be varied and denoted as h. A groove with rectangle cross section is inscribed on the top SiO_2 layer. The width and depth of groove are denoted as w_g and h_g, respectively. (b) the effective refractive indices of TE-BSW and TM-BSW modes versus the thickness h of top SiO_2 layer.

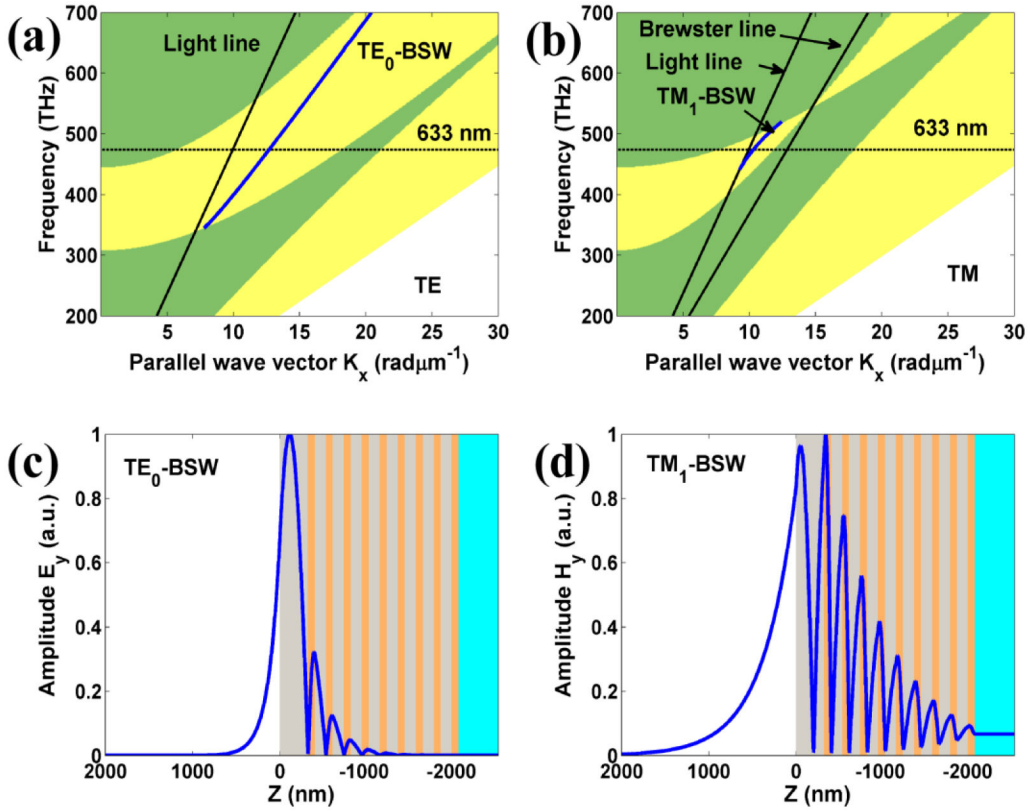

FIG. 2.

The projected band structure of the dielectric multilayer for (a) TE polarization, (b) TM polarization. The yellow zone denotes the stop band. The blue solid lines denote the dispersion curves for BSW with the thickness h =320 nm. (c) The electric field distribution for TE_0-BSW. (d) The magnetic field distribution for TM_1-BSW. The field distributions are calculated at the wavelength 633 nm.

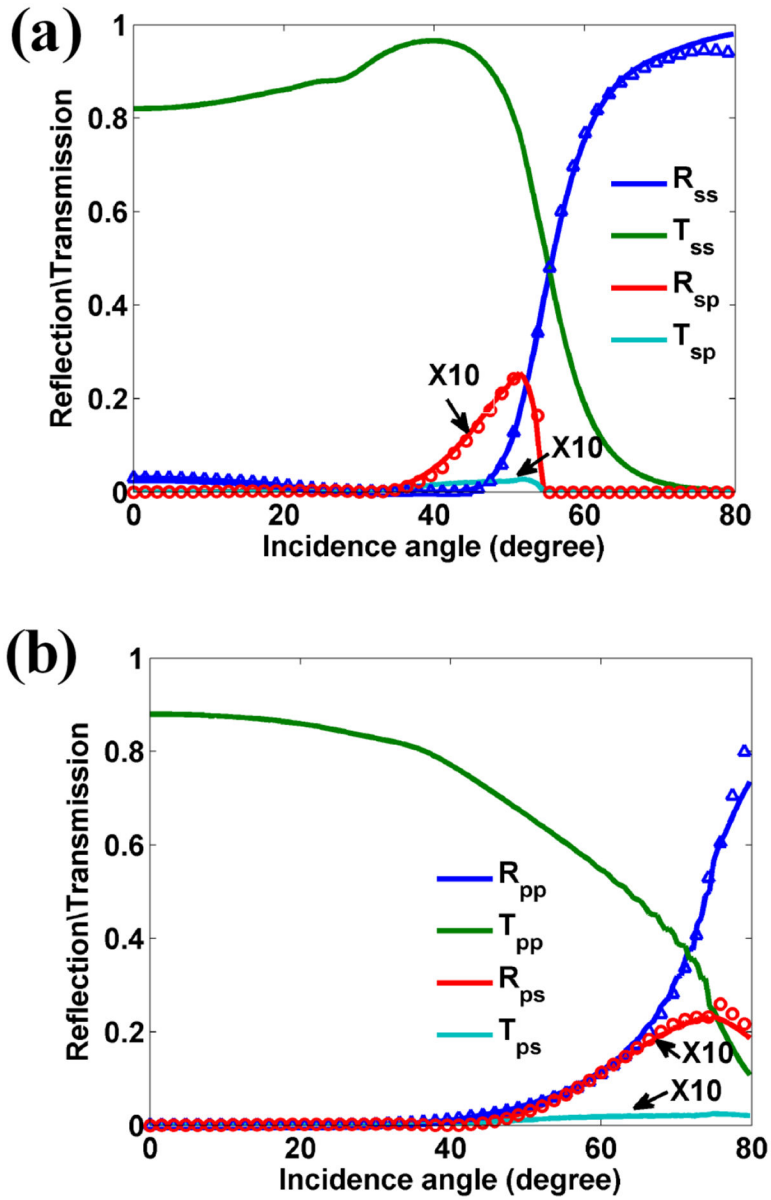

FIG. 3.

(a) The reflection (R_{ss}), transmission (T_{ss}) and polarization transformation (R_{sp} and T_{sp}) intensities of TE_0-BSW versus the angle of incidence. (b) The reflection (R_{pp}), transmission (T_{pp}) and polarization transformation (R_{ps} and T_{ps}) intensities of TM_1-BSW versus the angle of incidence. The signs with triangle and circle denote the results obtained from FDFD method. In simulation, the top layer's thickness h = 320 nm, the width w_g and depth h_g of the groove are 400 nm and 150 nm, respectively. The intensities of R_{sp}, T_{sp}, R_{ps} and T_{ps} are magnified by a factor of 10. The incident wavelength of the light in vacuum is 633 nm.

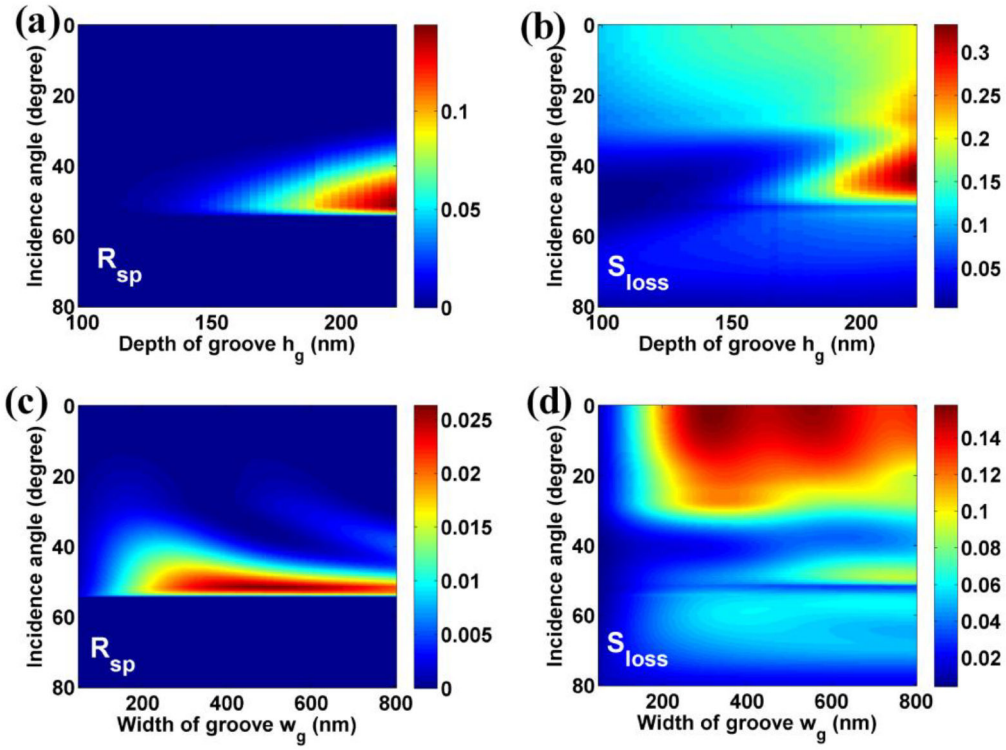

FIG. 4.

The influences of geometrical parameters of groove on the polarization transformation of BSW. (a) the polarization transformation intensity R_{sp}, and (b) the scattering loss of TE_0-BSW as a function of incidence angle and the depth of groove. The width of groove is fixed at 400 nm. As the depth of groove is fixed at 150 nm, (c) the polarization transformation intensity R_{sp}, and (d) the scattering loss of TE_0-BSW as a function of incidence angle and the width of groove.

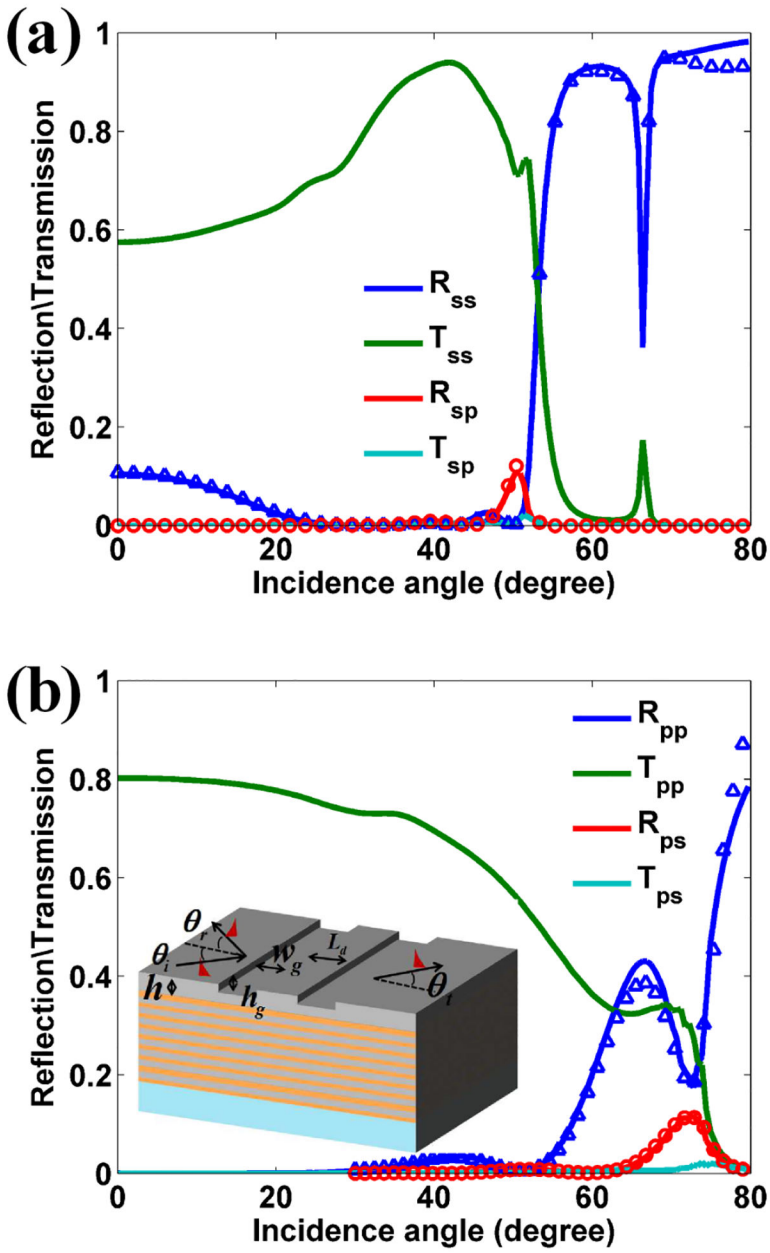

FIG. 5.

Reflection, transmission and polarization transformation intensities versus the incidence angle for (a) the incident wave is TE_0-BSW, (b) the incident wave is TM_1-BSW. The signs with triangle and circle denote the results obtained from FDFD method. Here, two grooves with separation distance L_d are inscribed in the top SiO_2 layer. The wavelength is 633 nm. The thickness of top layer is 320 nm. The width w_g and the depth h_g of groove are 400 nm and 150 nm, respectively. The separation distance L_d between the grooves is 400 nm.

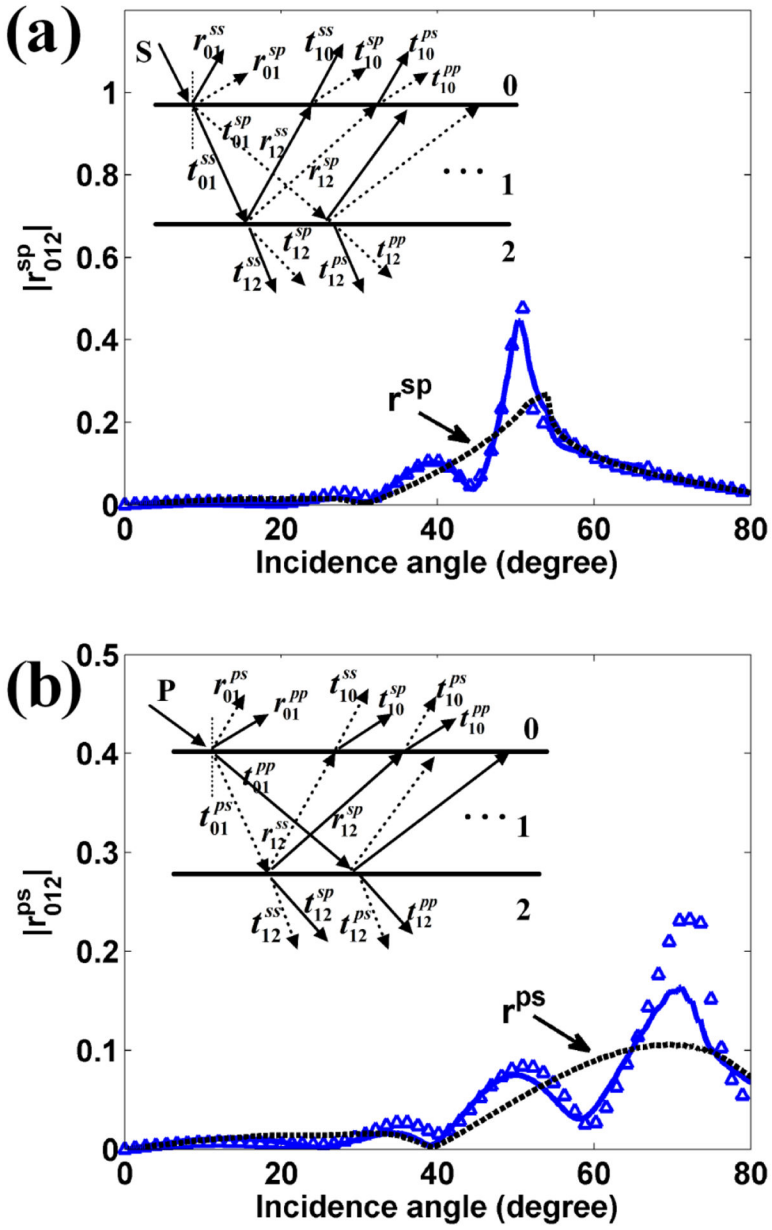

FIG. 6.

The amplitude of polarization transformation coefficients as a function of the incidence angle (a) r_{012}^{sp} for the polarization transformation of TE_0-BSW to TM_1-BSW, (b) r_{012}^{ps} for the polarization transformation of TM_1-BSW to TE_0-BSW. The solid lines denote the results obtained from Eq. (4), and the triangles denote the results obtained from the mode-matching method. The black dotted line denotes the polarization transformation coefficient of BSW for a single groove. The insets in the figure describe the simplified model of multiple reflection of BSW between the two grooves.

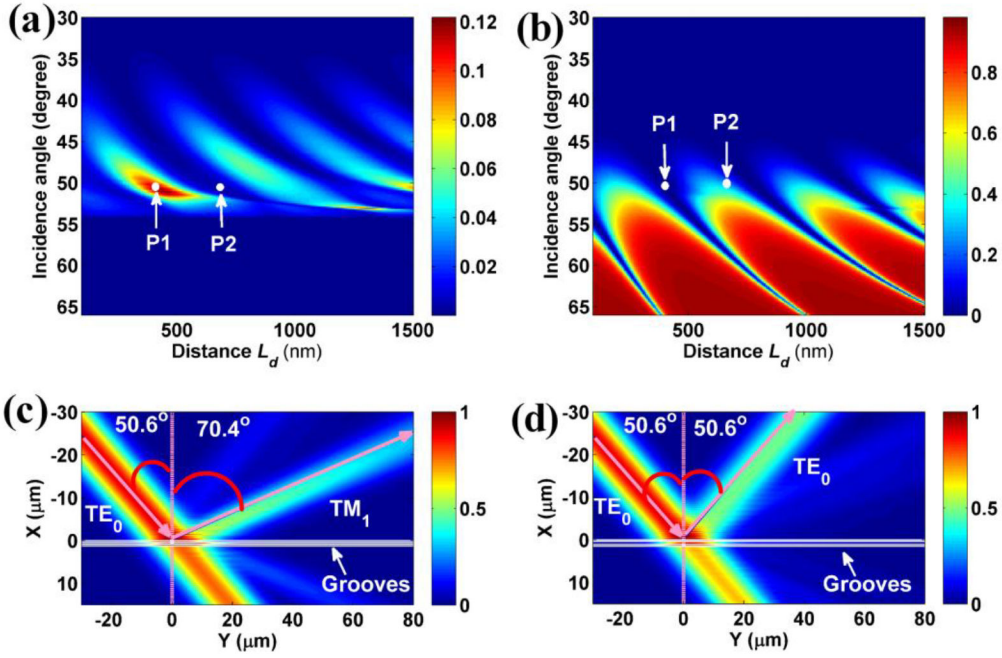

FIG. 7.

(a) Polarization transformation intensity R_{sp} and (b) the reflection intensity R_{ss} of TE_0-BSW versus the incidence angle and the separation distance L_d between grooves. The incidence angle of TE_0-BSW is fixed at 50.6°. The electric field intensity distributions for different separation distance (c) L_d = 410 nm, (d) L_d = 680 nm. The wavelength of the incident light in vacuum is 633 nm.

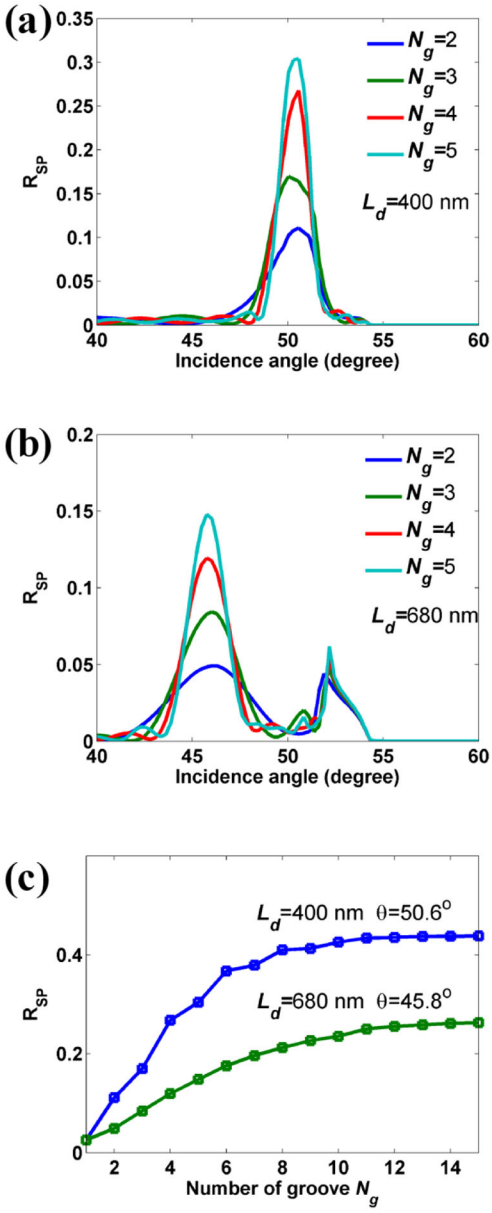

FIG. 8.

Polarization transformation intensity R_{sp} as a function of incidence angle with different numbers of grooves. The separation distance L_d between grooves is (a) 400 nm, (b) 680 nm. (c) The maximum transformation intensity R_{sp} versus the number of grooves N_g at the different separation distance L_d.